International Journal of Heat and Mass Transfer 52 (2009) 4510–4518

Contents lists available at ScienceDirect

International Journal of Heat and Mass Transfer

journal homepage: www.elsevier.com/locate/ijhmt

Immersed boundary method for the simulation of flows with heat transfer

Zeli Wang, Jianren Fan *, Kun Luo, Kefa Cen

State Key Laboratory of Clean Energy Utilization, Zhejiang University, Hangzhou 310027, PR China

ARTICLE INFO

Article history:
Received 24 July 2008
Received in revised form 10 March 2009
Accepted 16 March 2009
Available online 6 May 2009

Keywords:
Immersed boundary method
Direct forcing scheme
Direct heat source scheme
Heat transfer

ABSTRACT

In the present paper a direct heat source scheme is proposed to let the temperature at the immersed boundary satisfy the temperature Dirichlet boundary condition. And the explicit interactive process of the direct heat source scheme called multi-direct heat source scheme is applied to ensure the satisfaction of the temperature Dirichlet boundary condition at the immersed boundary. The second-order spacial accuracy of the solver is confirmed by simulating the Taylor–Green vortices. The simulations of natural convection between concentric cylinders, and flow past a stationary circular cylinder are conducted to validate the accuracy of present method on solving heat transfer problems. And the computation of flow past a staggered tube bank with heat transfer is conducted to verify the capability of present method on solving complex geometries problems.

1. Introduction

The flow past bluff bodies with convective heat transfer is widely existed in industry applications. The understanding of the characteristics of the convective heat transfer on bluff bodies is of great important in engineering. Experiments have been done to obtain the empirical correlations about the Nusselt number [1,6]. As the development of computer, many numerical studies on the convective heat transfer for the flow past bluff bodies have been done. Chang et al. [2] applied the finite-element method to study the heat transfer from a cylinder to a Newtonian fluid in laminar flow. Rosales et al. [5] numerically investigated the unsteady laminar flow and heat transfer characteristics from square cylinders located in a channel with a fully developed inlet velocity profile. Bagchi et al. [7] studied the flow and heat transfer past a sphere in a uniform flow with direct numerical solution in spherical coordinates. The body-fitted coordinates approach to solve flow past bluff bodies will increase the difficult in mesh generation. For the simulations of the oscillating or moving bluff bodies, the adapting mesh of the varying positions of the bluff bodies leads to tremendous computational cost. To overcome these problems, some computational techniques based on fixed Cartesian coordinates are proposed such as the distributed Lagrange multiplier/fictitious domain method [12], immersed interface method [13] and immersed boundary method [14].

The immersed boundary method originally proposed by Peskin [14] has attracted considerable interest in the last few years [15]. In Peskin's case, the singular force on the Lagrangian coordinates at the immersed boundary was exerted on the flow field via Dirac delta function. And for the sake of calculating the mutual interactions between solid boundary and fluid, some forcing schemes are proposed. Goldstein et al. [16] proposed a feedback forcing scheme to iteratively determined the magnitude of the force to let the velocity on the immersed boundary satisfy the no-slip boundary condition. Saiki et al. [17] applied this feedback forcing scheme to compute the flow past a stationary and oscillating circular cylinder successfully. Fadlun et al. [18] proposed a direct forcing scheme to calculate the interaction force between immersed boundary and fluid. The velocity at the points which are close to the immersed boundary is simply set at every time-step. And it seems like applying an equivalent forcing term to the Navier–Stokes equations. Uhlmann [19] applied the direct forcing with immersed boundary to study the particulate flows in multiphase system. The approach proposed by Uhlmann [19] incorporates the regularized delta function into a direct formulation of the fluid–solid interaction force to allow for a smooth transfer between the Eulerian girds and the Lagrangian points. Wang et al. [20] proposed a multi-direct forcing scheme to compute the interaction between the immersed boundary surface and fluid. The immersed boundary method with multi-direct forcing scheme proposed by Wang et al. [20] is based on the direct forcing scheme proposed by Fadlun et al. [18] and the smooth transfer method applied by Uhlmann [19] to iteratively reinforce the satisfaction of the no-slip boundary condition on the immersed surface.

The studies of the immersed boundary method mainly focus on solving the flow problems and seldom on heat transfer problems. Yoon et al. [3] applied the immersed-boundary finite volume method to investigate two-dimensional laminar fluid flow and heat transfer past a circular cylinder near a moving wall with. Kim et al. [10] used the immersed boundary method to study the natural convection induced by a temperature difference between a cold outer square enclosure and a hot inner circular cylinder numerically. Feng et al. [11] applied the immersed boundary meth-

* Corresponding author. Tel.: +86 571 87951764.
E-mail address: fanjr@zju.edu.cn (J. Fan).

0017-9310/$ - see front matter © 2009 Elsevier Ltd. All rights reserved.
doi:10.1016/j.ijheatmasstransfer.2009.03.048

Nomenclature

C_d	drag coefficient
c	parameter of outflow boundary condition
c_P	heat capacity
d_h	temporary parameter in Eq. (20)
$\boldsymbol{F}$	force exerted on the Lagrangian point
$\boldsymbol{f}$	external force
Gr	Grashof number
$\mathbf{g}$	characteristic acceleration of gravity
h	Eulerian grid size
k	thermal conductivity coefficient of fluid
L	characteristic length of flow field
L_w	wake length
l	norm error
m	tube sequence
N	number of Lagrangian points
N_D	number of total tubes
N_{Tr}	number of tubes in transverse direction
N_X, N_Y	total mesh points in x and y direction, respectively
NF_E	times of exerting multi-direct heat source
NF_M	times of exerting multi-direct forcing
Nu	Nusselt number
n	time level
P	pressure of fluid
Pe	Peclet number
Pr	Prandtl number
Q	heat source exerted on the Lagrangian point
q	heat source
R	radius of cylinder
Ra	Rayleigh number
Re	Reynolds number
r	temporary parameter in Eq. (21)
S_{Tr}	dimensionless transverse distance between two consecutive tubes
T	flow temperature
t	time
Δt	time step
U	characteristic velocity of flow field
$\boldsymbol{u}$	velocity of fluid
ΔV	discrete volume
$\boldsymbol{x}$	position of Eulerian mesh

Greek letters

Ω	whole computational domain
α	temporary parameter in Eqs. (22) and (27)
β	thermal expansion coefficient
ρ	fluid density
μ	viscosity of fluid
θ	angle measured from stagnation point
δ	Dirac delta function
δ_h	discrete Dirac delta function

Subscript

0	far-field parameter
1,2	count number
i	inter cylinder parameter
k	parameter defined on Lagrangian point
L	desired parameter
o	outer cylinder parameter
out	outflow boundary parameter
P	domain of immersed boundary
S	solid body parameter
T	temperature parameter
u	parameter in horizontal direction
v	parameter in vertical direction

Superscript

$\sim$	dimensionless parameter
$\langle\ \rangle$	average parameter

od with a difference method to study the thermal convection in particulate flows.

In the present paper, the immersed boundary method with finite difference scheme is applied to solve heat transfer problem. A direct heat source scheme is proposed to let the temperature at the immersed boundary satisfied the temperature Dirichlet boundary condition. And the explicit interactive process of the direct heat source scheme called multi-direct heat source scheme is applied to ensure the satisfaction of the temperature Dirichlet boundary condition at the immersed boundary. And the multi-direct forcing scheme proposed by Wang et al. [20] is applied to ensure the satisfaction of the no-slip velocity boundary condition at the immersed boundary. The paper is organized as follows. Section 2 introduces the numerical schemes for the momentum and energy coupling between fluid and solid boundary. Some numerical experiments are done to validate the accurate of the multi-direct heat source scheme which compose Section 3. And Section 4 is the summaries and conclusions.

2. Numerical schemes

2.1. Governing equations for fluid flow

The dimensionless governing equations for incompressible flows in the entire computational domain Ω with thermal convection are:

$$\nabla \cdot \tilde{\boldsymbol{u}} = 0 \tag{1}$$

$$\frac{\partial \tilde{\boldsymbol{u}}}{\partial \tilde{t}} + \tilde{\boldsymbol{u}} \cdot \nabla \tilde{\boldsymbol{u}} = -\nabla \tilde{P} + \frac{1}{\mathrm{Re}} \nabla^2 \tilde{\boldsymbol{u}} + \frac{Gr}{\mathrm{Re}^2} \cdot \tilde{T} \cdot \tilde{\boldsymbol{g}} + \tilde{\boldsymbol{f}} \tag{2}$$

$$\frac{\partial \tilde{T}}{\partial \tilde{t}} + \tilde{\boldsymbol{u}} \cdot \nabla \tilde{T} = \frac{1}{Pe} \nabla^2 \tilde{T} + \tilde{q} \tag{3}$$

where $\tilde{\boldsymbol{u}}$ is the dimensionless velocity of fluid, $\tilde{P}$ is the dimensionless pressure. Re is the Reynolds number defined as $\mathrm{Re} = \frac{\rho_0 \cdot U \cdot L}{\mu}$. Here, U is the characteristic velocity and L is the characteristic length of flow field, μ is the viscosity of fluid, ρ_0 is the density of fluid. Gr is the Grashof number defined as $Gr = \frac{g \cdot \beta \cdot (T_S - T_0) \cdot L^3 \cdot \rho_0^3}{\mu^2}$ with characteristic acceleration of gravity g, the coefficient of thermal expansion β, the temperature of immersed body T_S, and the far-field temperature T_0. Pe is the Peclet number defined as $Pe = \mathrm{Re} \cdot \mathrm{Pr}$, and Pr is the Prandtl number which is defined as $\mathrm{Pr} = \frac{c_P \cdot \mu}{k}$, where c_P is the heat capacity and k is the coefficient of thermal conductivity. The dimensionless temperature is defined as $\tilde{T} = \frac{T - T_0}{T_S - T_0}$.

In momentum equations (2), the dimensionless external force $\tilde{\boldsymbol{f}}$ which is the mutual interaction force between fluid and immersed boundary is expressed as following:

$$\tilde{\boldsymbol{f}}(\boldsymbol{x}) = \int_{\Omega_P} \boldsymbol{F}_k(\boldsymbol{x}_k) \cdot \delta(\boldsymbol{x} - \boldsymbol{x}_k) d\boldsymbol{x}_k \tag{4}$$

where Ω_P is the domain of the immersed boundary, $\delta(\boldsymbol{x} - \boldsymbol{x}_k)$ is the Dirac delta function, $\boldsymbol{x}_k$ is the position of the Lagrangian points set at

the immersed boundary, $\boldsymbol{x}$ is position of the computational Eulerian mesh and $\boldsymbol{F}_k(\boldsymbol{x}_k)$ is the force exerted on the Lagrangian point $\boldsymbol{x}_k$. Similarly in energy equation (3), the dimensionless external heat source $\tilde{q}$ which is the mutual interaction energy between fluid and immersed boundary is expressed as following:

$$\tilde{q}(\boldsymbol{x}) = \int_{\Omega_p} Q_k(\boldsymbol{x}_k)\cdot\delta(\boldsymbol{x}-\boldsymbol{x}_k)d\boldsymbol{x}_k \tag{5}$$

where $Q_k(\boldsymbol{x}_k)$ is the heat source on the Lagrangian point $\boldsymbol{x}_k$ at the immersed boundary.

2.2. Momentum and energy coupling scheme

2.2.1. Direct forcing scheme

For sake of sequence, the direct forcing and two-way coupling schemes are introduced first. In order to let the velocity on the Lagrangian points at the immersed boundary satisfy the no-slip boundary condition of velocity, a forcing $\boldsymbol{F}_k(\boldsymbol{x}_k)$ is imposed on the Lagrangian point to modify its velocity equal the desired velocity $\boldsymbol{u}_L$ at the immersed boundary. The forcing $\boldsymbol{F}_k(\boldsymbol{x}_k)$ is determined as follows.

From the momentum equation (Eq. (2)) of the flow field, one can get

$$\begin{aligned}\tilde{\boldsymbol{f}} &= \frac{\partial\tilde{\boldsymbol{u}}}{\partial\tilde{t}} + \tilde{\boldsymbol{u}}\cdot\nabla\tilde{\boldsymbol{u}} + \nabla\tilde{P} - \frac{1}{\mathrm{Re}}\nabla^2\tilde{\boldsymbol{u}} - \frac{Gr}{\mathrm{Re}^2}\cdot\tilde{T}\cdot\tilde{\boldsymbol{g}} = \frac{\partial\tilde{\boldsymbol{u}}}{\partial\tilde{t}} - \boldsymbol{rhsu}\\ &= \frac{\tilde{\boldsymbol{u}}^{n+1}-\tilde{\boldsymbol{u}}^{n}}{\Delta\tilde{t}} - \boldsymbol{rhsu}\end{aligned} \tag{6}$$

where n and $n+1$ represent two different time and

$$\boldsymbol{rhsu} = -\left(\tilde{\boldsymbol{u}}\cdot\nabla\tilde{\boldsymbol{u}} + \nabla\tilde{P} - \frac{1}{\mathrm{Re}}\nabla^2\tilde{\boldsymbol{u}} - \frac{Gr}{\mathrm{Re}^2}\cdot\tilde{T}\cdot\tilde{\boldsymbol{g}}\right) \tag{7}$$

And for the Lagrangian point xk at the immersed boundary, one can get

$$\boldsymbol{F}_k(\boldsymbol{x}_k) = \frac{\tilde{\boldsymbol{u}}_k^{n+1}-\tilde{\boldsymbol{u}}_k^{n}}{\Delta\tilde{t}} - \boldsymbol{rhsu}_k = \frac{\tilde{\boldsymbol{u}}_k^{n+1}-\hat{\boldsymbol{u}}_k}{\Delta\tilde{t}} + \frac{\hat{\boldsymbol{u}}_k-\tilde{\boldsymbol{u}}_k^{n}}{\Delta\tilde{t}} - \boldsymbol{rhsu}_k \tag{8}$$

where $\hat{\boldsymbol{u}}_k$ is a temporary parameter which satisfies the common momentum equation, that is

$$\frac{\hat{\boldsymbol{u}}_k-\tilde{\boldsymbol{u}}_k^{n}}{\Delta\tilde{t}} - \boldsymbol{rhsu}_k = 0 \tag{9}$$

Therefore, the forcing exerted on the Lagrangian points at the immersed boundary is

$$\boldsymbol{F}_k(\boldsymbol{x}_k) = \frac{\tilde{\boldsymbol{u}}_k^{n+1}-\hat{\boldsymbol{u}}_k}{\Delta\tilde{t}} = \frac{\boldsymbol{u}_L-\hat{\boldsymbol{u}}_k}{\Delta\tilde{t}} \tag{10}$$

Under the effect of the forcing, the velocity on the Lagrangian point $\boldsymbol{x}_k$ at $n+1$ time $\boldsymbol{u}_k^{n+1}$ can be modified to the desired velocity $\boldsymbol{u}_L$. The forcing is direct in the sense that the desired value of velocity is imposed directly on the boundary without any dynamical process [18] and the forcing is based upon the law of conservation [21].

2.2.2. Direct heat source scheme

Considering the Dirichlet boundary condition of temperature at the immersed boundary, the immersed boundary has a temperature T_L. In order to let the temperature at the immersed boundary equal T_L or in other words, let the temperature on the Lagrangian points at the immersed boundary satisfy the Dirichlet boundary condition of temperature, a heat source $Q_k(\boldsymbol{x}_k)$ is imposed on the Lagrangian point to modify its temperature equal the desired temperature T_L at the immersed boundary. The heat source $Q_k(\boldsymbol{x}_k)$ is determined as follows.

From the energy equation (Eq. (3)) of the flow field, one can get

$$\tilde{q} = \frac{\partial\tilde{T}}{\partial\tilde{t}} + \tilde{\boldsymbol{u}}\cdot\nabla\tilde{T} - \frac{1}{Pe}\nabla^2\tilde{T} = \frac{\partial\tilde{T}}{\partial\tilde{t}} - rhsT = \frac{\tilde{T}^{n+1}-\tilde{T}^{n}}{\Delta\tilde{t}} - rhsT \tag{11}$$

$$rhsT = -\left(\tilde{\boldsymbol{u}}\cdot\nabla\tilde{T} - \frac{1}{Pe}\nabla^2\tilde{T}\right) \tag{12}$$

And for the Lagrangian point $\boldsymbol{x}_k$ at the immersed boundary, one can get

$$Q_k(\boldsymbol{x}_k) = \frac{\tilde{T}_k^{n+1}-\tilde{T}_k^{n}}{\Delta\tilde{t}} - rhsT_k = \frac{\tilde{T}_k^{n+1}-\hat{T}_k}{\Delta\tilde{t}} - \frac{\hat{T}_k-\tilde{T}_k^{n}}{\Delta\tilde{t}} - rhsT_k \tag{13}$$

where $\hat{T}_k$ is a temporary parameter which satisfies the common energy equation, that is

$$\frac{\hat{T}_k-\tilde{T}_k^{n}}{\Delta\tilde{t}} - rhsT_k = 0 \tag{14}$$

Therefore, the heat source exerted on the Lagrangian points at the immersed boundary is

$$Q_k(\boldsymbol{x}_k) = \frac{\tilde{T}_k^{n+1}-\hat{T}_k}{\Delta\tilde{t}} = \frac{T_L-\hat{T}_k}{\Delta\tilde{t}} \tag{15}$$

Under the effect of the heat source in Eq. (15), the temperature on the Lagrangian point $\boldsymbol{x}_k$ at $n+1$ time $\tilde{T}_k^{n+1}$ can be modified to the desired velocity T_L. The scheme for heat source is direct in the sense that the desired temperature is imposed directly on the boundary without any dynamical process.

2.2.3. Momentum and energy coupling between fluid and immersed boundary

As described in Eqs. (4) and (5), the Dirac delta function is applied to spread the two-way coupling between Eulerian girds and Lagrangian points at the immersed boundary. The temporary velocity $\hat{\boldsymbol{u}}_k$ and temperature $\hat{T}_k$ on the Lagrangian point at the immersed boundary $\boldsymbol{x}_k$ are obtained from its surrounding Eulerian grids $\boldsymbol{x}$ for two-dimensional computation as following

$$\hat{\boldsymbol{u}}_k = \sum_{\boldsymbol{x}\in\Omega}\hat{\boldsymbol{u}}\cdot\delta_h(\boldsymbol{x}_k-\boldsymbol{x})\cdot h^2 \tag{16}$$

$$\hat{T}_k = \sum_{\boldsymbol{x}\in\Omega}\hat{T}\cdot\delta_h(\boldsymbol{x}_k-\boldsymbol{x})\cdot h^2 \tag{17}$$

where $\hat{\boldsymbol{u}}$ and $\hat{T}$ are also the temporary parameters on the Eulerian grids which satisfies the common momentum equation and common energy equation, respectively.

The effects of the forcing and heat source on the Lagrangian points which spread into the Eulerian grids are expressed as:

$$\tilde{\boldsymbol{f}}(\boldsymbol{x}) = \int_{\Omega_p}\boldsymbol{F}_k(\boldsymbol{x}_k)\cdot\delta(\boldsymbol{x}-\boldsymbol{x}_k)d\boldsymbol{x}_k = \sum_{k=1}^{N}\boldsymbol{F}_k(\boldsymbol{x}_k)\cdot\delta_h(\boldsymbol{x}-\boldsymbol{x}_k)\cdot\Delta V_k \tag{18}$$

$$\tilde{q}(\boldsymbol{x}) = \int_{\Omega_p} Q_k(\boldsymbol{x}_k)\cdot\delta(\boldsymbol{x}-\boldsymbol{x}_k)d\boldsymbol{x}_k = \sum_{k=1}^{N} Q_k(\boldsymbol{x}_k)\cdot\delta_h(\boldsymbol{x}-\boldsymbol{x}_k)\cdot\Delta V_k \tag{19}$$

where N is the number of Lagrangian points, and ΔV_k is the discrete volume for each Lagrangian point. The discrete volume for each Lagrangian point is $\Delta V_k = h\cdot\Delta s$ for 2D computation, where Δs is the curve distance between two neighboring Lagrangian points of the immersed boundary.

The discrete delta function is chosen as that of Griffith and Peskin [22] for two-dimensional computation.

$$\delta_h(\boldsymbol{x}-\boldsymbol{x}_k) = \frac{1}{h^2}d_h\left(\frac{x-x_k}{h}\right)\cdot d_h\left(\frac{y-y_k}{h}\right) \tag{20}$$

where $\boldsymbol{x} = (x,y), \boldsymbol{x}_k = (x_k,y_k), h$ is the Eulerian mesh size, and

$$d_h(r) = \begin{cases}\frac{1}{8}(3-2|r|+\sqrt{1+4|r|-4r^2}) & 0\le|r|<1\\ \frac{1}{8}(5-2|r|-\sqrt{-7+12|r|-4r^2}) & 1\le|r|<2\\ 0 & 2\le|r|\end{cases} \tag{21}$$

To solve the governing equations, the spatial derivatives are discretized using the fourth-order compact finite difference scheme [23] based on non-staggered grid. The pressure-Poisson equation derived by applying the divergence operator to the momentum equations replaces the continuity equation that is satisfied indirectly through the solution of the pressure equation. To reduce the cost of core memory in simulations, the temporal integration scheme [24] is applied. The computational algorithm is described as follows.

$$\tilde{\boldsymbol{u}}_{\alpha+1} = \tilde{\boldsymbol{u}}^n + \boldsymbol{rhsu}_\alpha \cdot \frac{\Delta\tilde{t}}{4-\alpha}, \quad \alpha = 0,1,2,3 \tag{22}$$

$$\hat{\boldsymbol{u}}_k = \sum_{x\in\Omega} \tilde{\boldsymbol{u}}_4 \cdot \delta_h(\boldsymbol{x}_k - \boldsymbol{x}) \cdot h^2 \tag{23}$$

$$\boldsymbol{F}_k(\boldsymbol{x}_k) = \frac{\boldsymbol{u}_L - \hat{\boldsymbol{u}}_k}{\Delta\tilde{t}} \tag{24}$$

$$\tilde{\boldsymbol{f}}(\boldsymbol{x}) = \sum_{k=1}^{N} \boldsymbol{F}_k(\boldsymbol{x}_k) \cdot \delta_h(\boldsymbol{x} - \boldsymbol{x}_k) \cdot \Delta V_k \tag{25}$$

$$\tilde{\boldsymbol{u}}^{n+1} = \tilde{\boldsymbol{u}}_4 + \tilde{\boldsymbol{f}}(\boldsymbol{x}) \cdot \tilde{\Delta}t \tag{26}$$

$$\tilde{T}_{\alpha+1} = \tilde{T}^n + rhsT_\alpha \cdot \frac{\Delta\tilde{t}}{4-\alpha}, \quad \alpha = 0,1,2,3 \tag{27}$$

$$\hat{T}_k = \sum_{\boldsymbol{x}\in\Omega} \tilde{T}_\alpha \cdot \delta_h(\boldsymbol{x}_k - \boldsymbol{x}) \cdot h^2 \tag{28}$$

$$Q_k(\boldsymbol{x}_k) = \frac{T_L - \hat{T}_k}{\Delta\tilde{t}} \tag{29}$$

$$\tilde{q}(\boldsymbol{x}) = \sum_{k=1}^{N} Q_k(\boldsymbol{x}_k) \cdot \delta_h(\boldsymbol{x} - \boldsymbol{x}_k) \cdot \Delta V_k \tag{30}$$

$$\tilde{T}^{n+1} = \tilde{T}_4 + \tilde{q}(\boldsymbol{x}) \cdot \tilde{\Delta}t \tag{31}$$

$$\nabla^2\tilde{P} = -\nabla\cdot(\tilde{\boldsymbol{u}}\cdot\nabla\tilde{\boldsymbol{u}}) - \frac{\partial(\nabla\cdot\tilde{\boldsymbol{u}})}{\partial t} + \nabla\cdot\tilde{\boldsymbol{f}} + \frac{Gr}{\mathrm{Re}^2}\nabla\cdot(\tilde{T}\cdot\tilde{\boldsymbol{g}}) \tag{32}$$

2.2.4. Multi-direct forcing and multi-direct heat source processes

The formulation of direct forcing scheme and direct heat source scheme is based on a single Lagrangian point. When applying direct forcing and direct heat source on a group of interactional Lagrangian points and spreading the effect of forcing and heat source to Eulerian grids through the interpolation/extrapolation scheme (or the Dirac delta function), the direct forcing scheme and direct heat source scheme will not be so effectively. Different schemes of discrete delta function can lead to different results. The velocities and temperature on the Lagrangian points may not satisfy the Dirichlet boundary condition very well during the process of interpolation to obtain the simulated velocity and temperature on the Lagrangian points and extrapolation to spread the forcing and heat source effect to its surrounding Eulerian grids. The multi-direct forcing/heat source scheme can handle this problem. Under the effect of the multi-direct forcing the velocity at the immersed boundary can satisfy the no-slip boundary condition immediately and accurately as discussed by Wang et al. [20] and Luo et al. [25]. And the temperature on the Lagrangian points at the immersed boundary can satisfy the Dirichlet boundary condition either which will be validated in Section 3. The multi-direct forcing and multi-direct heat source processes are described in detail as follows.

By solving Eqs. (22)–(26), the velocity of the whole flow field $\tilde{\boldsymbol{u}}_1^{n+1}$ is obtained where $n+1$ is the time level and the subscript 1 represents exerting the direct forcing at the immersed boundary for the first time. Then the velocity on the Lagrangian point is

$$\hat{\boldsymbol{u}}_{k,1} = \sum_{x\in\Omega} \tilde{\boldsymbol{u}}_1^{n+1} \cdot \delta_h(\boldsymbol{x}_k - \boldsymbol{x}) \cdot h^2 \tag{33}$$

The best result is $\hat{\boldsymbol{u}}_{k,1} = \boldsymbol{u}_L$, but always $\hat{\boldsymbol{u}}_{k,1} \neq \boldsymbol{u}_L$. Though the velocity at the immersed boundary can get close to the desired velocity after a long period of time, the no-slip boundary condition is still not satisfied very well. For the sake of getting the velocity on the Lagrangian point much close to the desired velocity, the direct forcing is exerted for the second time which makes

$$\boldsymbol{F}_{k,2}(\boldsymbol{x}_k) = \frac{\boldsymbol{u}_L - \hat{\boldsymbol{u}}_{k,1}}{\Delta\tilde{t}} \tag{34}$$

Then the forcing is spread from the Lagrangian points to the Eulerian grids through the Dirac delta function

$$\tilde{\boldsymbol{f}}_2(\boldsymbol{x}) = \sum_{k=1}^{N} \boldsymbol{F}_{k,2}(\boldsymbol{x}_k) \cdot \delta(\boldsymbol{x} - \boldsymbol{x}_k) \cdot \Delta V_k \tag{35}$$

After exerting the direct forcing for the second time, the velocity of the whole flow field becomes

$$\tilde{\boldsymbol{u}}_2^{n+1} = \tilde{\boldsymbol{u}}_1^{n+1} + \tilde{\boldsymbol{f}}_2(\boldsymbol{x}) \cdot \Delta\tilde{t} \tag{36}$$

Thus the velocity on the Lagrangian point at the immersed boundary becomes

$$\hat{\boldsymbol{u}}_{k,2} = \sum_{x\in\Omega} \tilde{\boldsymbol{u}}_2^{n+1} \cdot \delta(\boldsymbol{x}_k - \boldsymbol{x}) \cdot h^2 \tag{37}$$

The value of $\hat{\boldsymbol{u}}_{k,2}$ is expected to be closer to the desired velocity $\boldsymbol{u}_L$ than that of $\hat{\boldsymbol{u}}_{k,1}$. After NF_M times of this procedure during one time step, the velocity at the immersed boundary can get much close to the desired velocity. The total forcing exerting on each Lagrangian point $\boldsymbol{F}_k(\boldsymbol{x}_k)$ is the sum of the forcing exerting on each Lagrangian point for the whole NF_M times, that is:

$$\boldsymbol{F}_k(\boldsymbol{x}_k) = \sum_{i=1}^{NF_M} \boldsymbol{F}_{k,i}(\boldsymbol{x}_k) \tag{38}$$

Besides the multi-direct forcing, the multi-direct heat source process is proposed here. By solving Eqs. (27)–(30), the temperature of the whole flow field $\tilde{T}_1^{n+1}$ is obtained. Then the temperature on the Lagrangian point is

$$\hat{T}_{k,1} = \sum_{x\in\Omega} \tilde{T}_1^{n+1} \cdot \delta(\boldsymbol{x}_k - \boldsymbol{x}) \cdot h^2 \tag{39}$$

The direct heat source is exerted for the second time which makes

$$Q_{k,2}(\boldsymbol{x}_k) = \frac{T_L - \hat{T}_{k,1}}{\Delta\tilde{t}} \tag{40}$$

Then the heat source is spread from the Lagrangian points to the Eulerian grids through the Dirac delta function

$$\tilde{q}_2(\boldsymbol{x}) = \sum_{k=1}^{N} Q_{k,2}(\boldsymbol{x}_k) \cdot \delta_h(\boldsymbol{x} - \boldsymbol{x}_k) \cdot \Delta V_k \tag{41}$$

After exerting the direct heat source for the second time, the temperature of the whole flow field becomes

$$\tilde{T}_2^{n+1} = \tilde{T}_1^{n+1} + \tilde{q}_2(\boldsymbol{x}) \cdot \tilde{\Delta}t \tag{42}$$

And the temperature on the Lagrangian point at the immersed boundary is

$$\hat{T}_{k,2} = \sum_{x\in\Omega} \tilde{T}_2^{n+1} \cdot \delta(\boldsymbol{x}_k - \boldsymbol{x}) \cdot h^2 \tag{43}$$

The value of $\hat{T}_{k,2}$ is expected to be closer to the desired velocity T_L than that of $\hat{T}_{k,1}$. After NF_E times of this procedure during one time step, the temperature at the immersed boundary can get much close to the desired temperature.

The multi-direct forcing and multi-direct heat source processes for the calculation of the momentum and energy coupling between immersed boundary and fluid can be summarized as follows:

(1) Solving Eq. (22) to obtain the flow field $\tilde{\boldsymbol{u}}_1^{n+1}$.
(2) Solving Eq. (33) to get the velocity at the immersed boundary.
(3) Verifying the error between the calculated velocity at the immersed boundary and the desired velocity and the times of exerting direct forcing. If the error is larger than a desired value or the times is not reached the targeted times NF_M, the next time of direct forcing procedure is started. If the error is smaller than a desired value or the times is greater than the targeted times NF_M, then go to next.
(4) Solving Eq. (27) to get the temperature distribution in the whole computational domain.
(5) Solving Eq. (39) to get the temperature at the immersed boundary.
(6) Verifying the error between the calculated temperature at the immersed boundary and the desired temperature and the times of exerting direct heat source. If the error is larger than a desired value or the times is not reached the targeted times NF_E, the next time of direct heat source procedure is started. If the error is smaller than a desired value or the times is greater than the targeted times NF_E, then solving the pressure-Poisson equation (32) and beginning the next time loop.

3. Numerical implement and discussion

To validate the accuracy of method proposed in Section 2, we first calculate the Taylor–Green vortices problem which has an analytical solution. Then natural convection between concentric cylinders and the flow past a stationary circular cylinder are simulated with present method. At last the flow past a staggered tube bank with heat transfer are simulated to verify the capability of present method on solving complex geometries problems.

3.1. Taylor–Green vortices

In order to validate the multi-direct forcing effect and spatial accuracy of the present immersed boundary method with multi-direct forcing scheme, the case of two-dimensional decaying vortices with analytical solution (Eqs. (44)–(46)) is simulated.

$$\tilde{u}(\tilde{x},\tilde{y},\tilde{t}) = -\cos(\pi\cdot\tilde{x})\cdot\sin(\pi\cdot\tilde{y})\cdot\exp(-2\pi^2\tilde{t}/\mathrm{Re}) \tag{44}$$

$$\tilde{v}(\tilde{x},\tilde{y},\tilde{t}) = \sin(\pi\cdot\tilde{x})\cdot\cos(\pi\cdot\tilde{y})\cdot\exp(-2\pi^2\tilde{t}/\mathrm{Re}) \tag{45}$$

$$\tilde{p}(\tilde{x},\tilde{y},\tilde{t}) = -1/4[\cos(2\pi\cdot\tilde{x})+\cos(2\pi\cdot\tilde{y})]\exp(-4\pi^2\tilde{t}/\mathrm{Re}) \tag{46}$$

Kim et al. [4] calculated this problem in a quadrilateral embedded domain and Uhlmann [19] solved this case in an embedded circular domain. And here, we calculated this problem in an embedded circular domain with radius unity and centered at the whole computational domain $\Omega = [-1.5, 1.5]\times[-1.5, 1.5]$ with Re = 100. The boundary conditions for whole computational domain and desired velocity at the immersed boundary are given by Eqs. (44)–(46).

Fig. 1 shows the effect of multi-direct forcing exerting on the immersed boundary of the embedded circular for $\Delta\tilde{t} = 0.001$, $h = 1/64$ and at $\tilde{t} = 0.3$. The $l_{2,uv}$-norm is defined in Eq. (47) which can show the error between the desired velocity $\tilde{\boldsymbol{u}}_L = (\tilde{u}_L, \tilde{v}_L)$ and calculated velocity at the immersed boundary.

$$l_{2,uv} = \sqrt{\frac{\sum_{k=1}^{N}[(\tilde{u}_k-\tilde{u}_L)^2+(\tilde{v}_k-\tilde{v}_L)^2]}{N}} \tag{47}$$

where $\tilde{\boldsymbol{u}}_k = (\tilde{u}_k, \tilde{v}_k)$ is the velocity on kth Lagrangian point at the immersed boundary. The magnitude of $l_{2,uv}$-norm is decreased as the increment of the times NF_M of multi-direct forcing for momentum coupling between the fluid and the immersed boundary. This indicates the no-slip boundary condition of velocity at the immersed boundary is satisfied better with the multi-direct forcing scheme than that for the original direct forcing scheme ($NF_M = 1$). And $NF_M = 20$ will be applied in the following computation. The time cost of each iterative process of the multi-direct forcing in this case on a P4, 2.8 GHz CPU is 3.906×10^{-3} s corresponding to 5.466×10^{-2} and 5.859×10^{-2} s at one time step for solving the momentum equations and the Poisson equation, respectively. Considering a better satisfaction of the no-slip boundary at the immersed boundary, the time cost of the multi-direct forcing is acceptable.

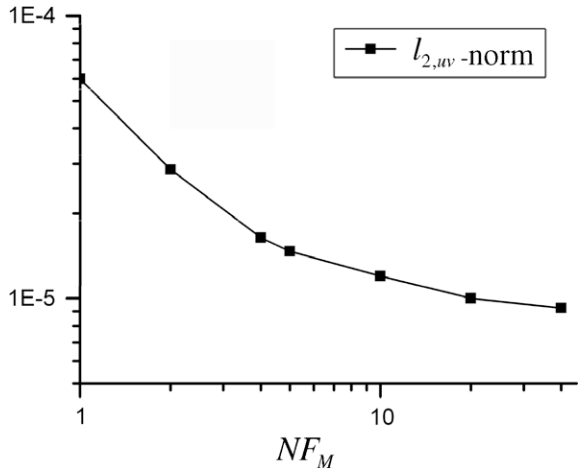

Fig. 1. Correlation between the $l_{2,uv}$-norm and the times of multi-direct forcing NF_M to show the effect of multi-direct forcing exerting on the immersed boundary of the embedded circular in the case of Taylor–Green vortices.

Fig. 2 shows the convergence of spatial accuracy for $\Delta\tilde{t} = 0.001$ and results at $\tilde{t} = 0.3$ with mesh size $h = 1/8, 1/16, 1/32, 1/64$ and $1/128$, and corresponding Lagrangian points are 56, 110, 220, 440 and 880, respectively. The $l_{1,u}$-norm and $l_{2,u}$-norm are defined in Eqs. (48) and (49), respectively.

$$l_{1,u} = \frac{1}{N_X N_Y}\sum_{k=1}^{N_X N_Y}|\tilde{u}_k^{numerical}-\tilde{u}_k^{exact}| \tag{48}$$

$$l_{2,u} = \sqrt{\frac{1}{N_X N_Y}\sum_{k=1}^{N_X N_Y}(\tilde{u}_k^{numerical}-\tilde{u}_k^{exact})^2} \tag{49}$$

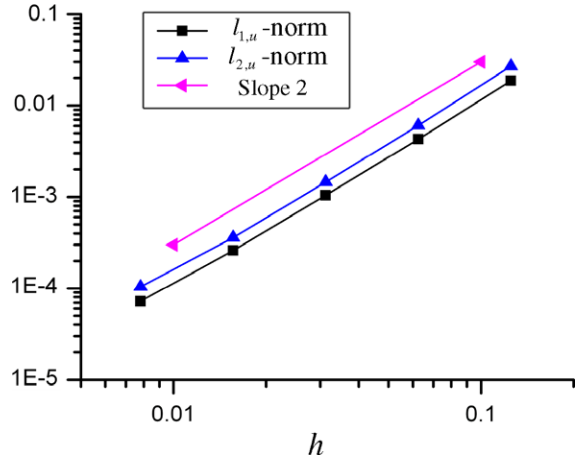

Fig. 2. Correlation of the $l_{1,u}$-norm and $l_{2,u}$-norm versus grid size to show the special convergence in the case of Taylor–Green vortices.

where N_X and N_Y are the total mesh points in x and y direction, respectively.

The $l_{1,u}$-norm and $l_{2,u}$-norm are decreased in slope 2 as the decrement of mesh size which corresponds to second-order convergence in spacial accuracy.

3.2. Natural convection between concentric cylinders

In this case natural convection in the annulus between horizontal concentric cylinders is simulated. The computational parameters are the same as Kuehn and Goldstein [28] and Gan et al. [29]. The inter cylinder has a radius $R_i = 0.625$ and temperature $\tilde{T}_i = 1$, while the outer cylinder has a radius $R_o = 1.625$ and temperature $\tilde{T}_o = 0$.. The schematic diagram for entire computational domain is shown in Fig. 3. The two concentric cylinders are place at (2.5, 2.5) and the size of whole computational domain is 5×5. Due to the difference of the radius of the two cylinders, the numbers of Lagrangian points at the immersed boundary are different. However, for the sake of convenience, the same number of Lagrangian points at the two immersed boundary is applied. The Peclet number is $Pe = 1$, the Prandtl number is Pr = 0.7, and the Rayleigh number is $Ra = 5 \times 10^4$, which is defined as $Ra = Gr \cdot \Pr$. The $NF_M = 20$ of multi-direct forcing is used and the effect of multi-direct heat source scheme will be analyzed.

Fig. 4 shows the correlation of $l_{2,T}$-norm defined in Eq. (50) and the times of direct heat source NF_E for temperature with mesh size $h = 1/64$, number of Lagrangian points on each cylinder $N = 736$ and time step $\Delta\tilde{t} = 0.001$. As the increment of the times of direct heat source NF_E, the $l_{2,T}$-norm decreases for the two cylinders. This indicates the computational value of temperature at the immersed boundary satisfied the desired temperature better for larger NF_E than that for smaller NF_E. And the multi-direct heat source process can reduce the error between the computational value of temperature and the desired value of temperature effectively.

$$l_{2,T} = \sqrt{\frac{\sum_{k=1}^{N}(\tilde{T}_k - T_L)^2}{N}} \tag{50}$$

The counter of temperature distribution is shown in Fig. 5. And Fig. 6 shows the temperature distribution between the two cylinders at $\theta = 120^\circ$ and the comparison with the results from Kuehn et al. [28], Gan et al. [29]. A good agreement is obtained.

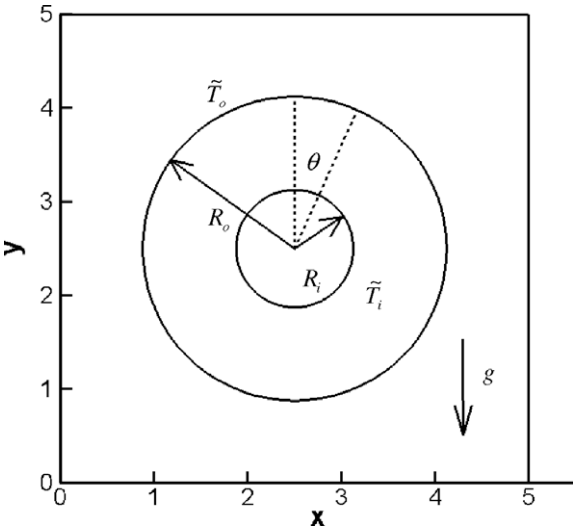

Fig. 3. Schematic diagram of whole computational domain for the case of natural convection between concentric cylinders.

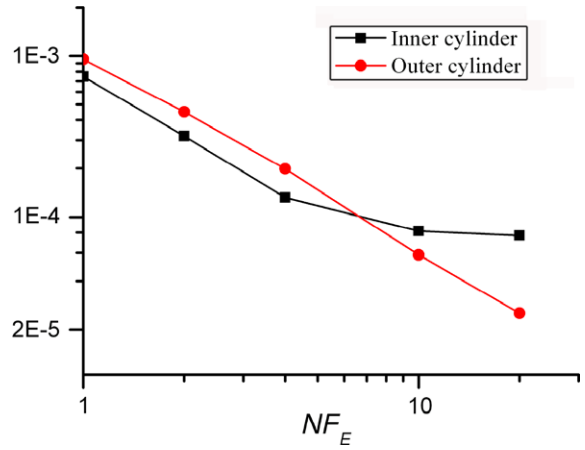

Fig. 4. Correlation of $l_{2,T}$-norm defined in Eq. (50) versus the times of direct heat source NF_E for temperature with mesh size $h = 1/64$, number of Lagrangian points on each cylinder $N = 736$ and time step $\Delta\tilde{t} = 0.001$.

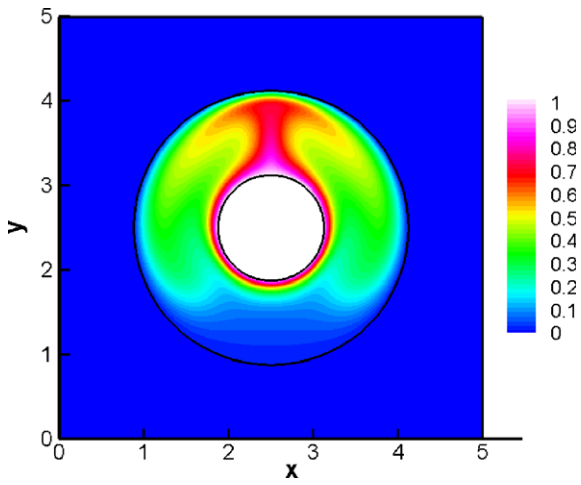

Fig. 5. Counter of temperature distribution for the case of Natural convection between concentric cylinders.

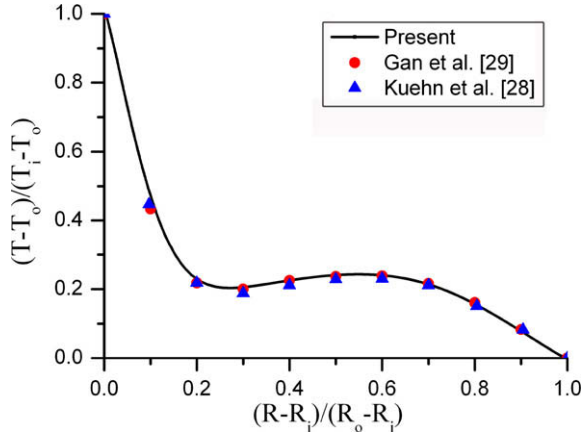

Fig. 6. Temperature distribution between the two cylinders at $\theta = 120^\circ$ and the comparison with the results from Kuehn et al. [28], Gan et al. [29].

Fig. 7 shows the convergence of the $l_{1,T}$-norm and $l_{2,T}$-norm defined in Eqs. (51) and (52) with mesh sizes $h = 1/16, 1/32$ and $1/64$ in the magnitude of temperature field relative to the "bench-

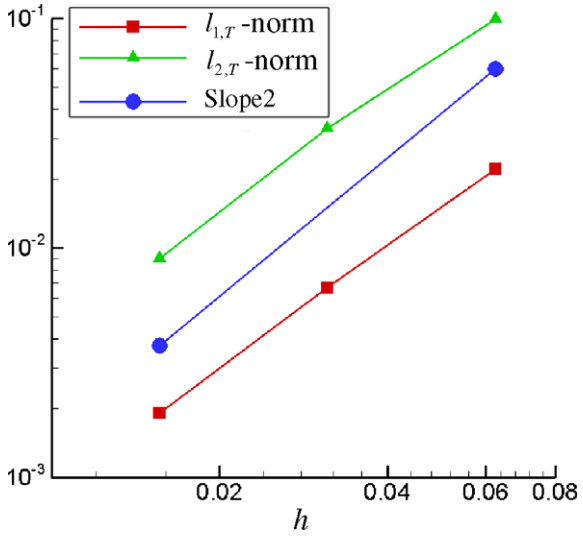

Fig. 7. Convergence of the $l_{1,T}$-norm and $l_{2,T}$-norm with mesh sizes $h = 1/16, 1/32$ and $1/64$ in the magnitude of temperature field relative to the "benchmark" solution of temperature field obtained on mesh size $h = 1/128$.

mark" solution of temperature field obtained on grid size $h = 1/128$.

$$l_{1,T} = \frac{1}{N_X N_Y} \sum_{k=1}^{N_X N_Y} \left| \tilde{T}_k^{numerical} - \tilde{T}_k^{benchmark} \right| \tag{51}$$

$$l_{2,T} = \sqrt{\frac{1}{N_X N_Y} \sum_{k=1}^{N_X N_Y} (\tilde{T}_k^{numerical} - \tilde{T}_k^{benchmark})^2} \tag{52}$$

The $l_{1,T}$-norm and $l_{2,T}$-norm is decreased in slope 2 as the decrement of mesh size which corresponds to second-order convergence in temperature field.

3.3. Flow past a stationary circular cylinder with heat transfer

For the flow past a stationary circular cylinder with heat transfer, Dennis et al. [30] solved this problem by obtaining solutions of the heat transfer equation based on the correct velocity distribution in the field of flow according to the full Navier–Stokes equations. Chang et al. [2] applied the finite-element method and body-fitted mesh to solve this problem. Gan et al. [29] applied finite-element method and the arbitrary Lagrangian–Eulerian technique to solve the forced convection around a stationary circular cylinder. And here, we compute the same case as Dennis et al. [30], Chang et al. [2] and Gan et al. [29].

The schematic of computational domain is shown in Fig. 8. The non-dimensional computational domain is 28×20 when takes the diameter of circular cylinder as the characteristics length. At the inflow boundary, $\tilde{u} = 1, \tilde{v} = 0, \tilde{T} = 0$ are given where $\tilde{\boldsymbol{u}} = (\tilde{u}, \tilde{v})$. At the boundaries in y direction, $\frac{\partial \tilde{T}}{\partial y} = 0, \frac{\partial \tilde{u}}{\partial y} = 0, \tilde{v} = 0$ are given. And at the outflow boundary, the non-reflecting condition [31] are applied $\frac{\partial \tilde{\boldsymbol{u}}}{\partial \tilde{t}} + c\frac{\partial \tilde{\boldsymbol{u}}}{\partial x} = 0, \frac{\partial \tilde{T}}{\partial \tilde{t}} + c\frac{\partial \tilde{T}}{\partial x} = 0$. At the immersed boundary of the circular cylinder, the desired velocity and desired temperature are $\tilde{u} = 0, \tilde{v} = 0, \tilde{T} = 1$, respectively. The Reynolds number is Re = 20, the Prandtl number is Pr = 0.73, and the Grashof number is $Gr = 0$. The times of multi-direct forcing scheme and the multi-direct heat source scheme are the same $NF_M = NF_E = 20$. The time step is $\Delta\tilde{t} = 0.0005$, the mesh size is $h = 1/96$ and the number of Lagrangian points at the immersed boundary is $N = 332$.

Fig. 9 shows the comparison of local Nusselt number near the cylinder from the results of Chang et al. [2], Gan et al. [29], Dennis et al. [30] and present results. A good agreement is obtained. The

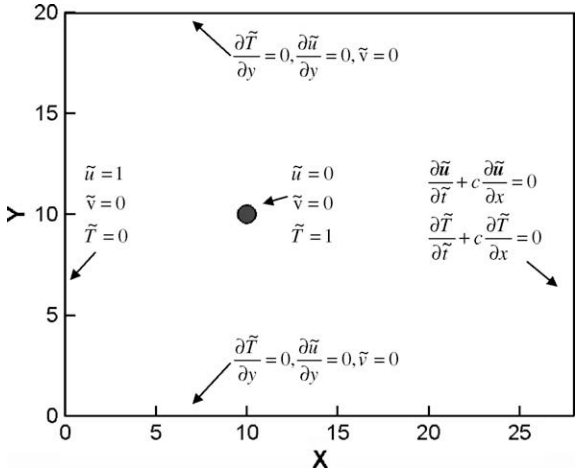

Fig. 8. Schematic view of computational domain for the case of flow past a stationary with heat transfer.

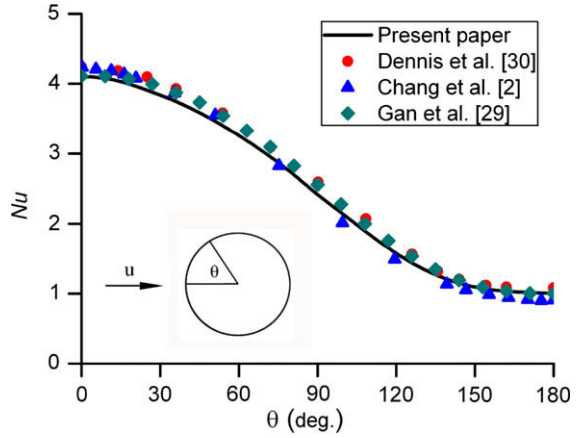

Fig. 9. Comparison of local Nusselt number near the cylinder between the results of Chang et al. [2], Gan et al. [29], Dennis et al. [30] and present results.

streamline accompanied with temperature distribution is shown in Fig. 10. Table 1 shows the drag coefficient C_d and wake length L_w (measured from rear end of cylinder) of present results comparing with the experimental result of Tritton [32] and numerical results of Dennis et al. [26] and Ye et al. [27]. Our results are in good agreement with previous experimental and numerical results.

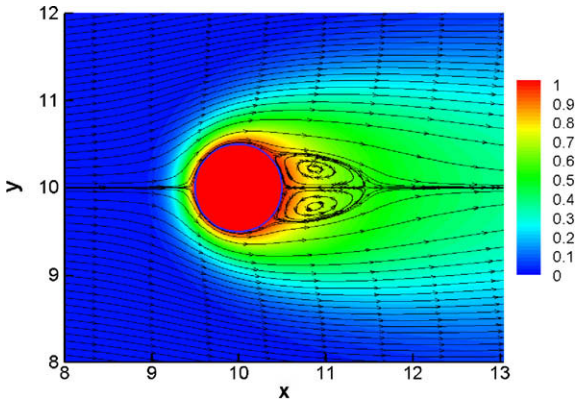

Fig. 10. Distribution of streamline accompanied with temperature field at the surface of the cylinder.

Table 1
Comparison of drag coefficient C_d and wake length L_w.

Re = 20	C_d	L_w
Present	2.18	0.946
Tritton [32]	2.22	–
Dennis et al. [26]	2.05	0.94
Ye et al. [27]	2.03	0.92

3.4. Flow past a staggered tube bank with heat transfer

The flow past a staggered tube bank with convective heat transfer is computed to verify the ability of present methods to complex geometries. The staggered tube bank is composed by 77 cylinders immersed in a rectangular domain. The whole computational domain is 18×22 when takes the diameter of cylinder as the characteristics length. The distances between two rows in streamwise direction and transverse direction are the same which is 2. And the other computational parameters including the Reynolds number, the Prandtl number, the Grashof number, the times of NF_M and NF_E, the time step, the mesh size and the number of the Lagrangian points used for a cylinder are the same as these in Section 3.3. The inflow and outflow boundary conditions are the same as these in Section 3.3 and the no-slip boundary condition is imposed on the boundaries in transverse direction.

The distribution of temperature field is shown in Fig. 11. The average Nusselt number can be obtained from Eq. (53) by using energy balance.

$$\langle Nu \rangle = -\mathrm{RePr}\frac{N_{Tr}S_{Tr}}{\pi N_D}\ln(1-\langle \tilde{T}_{out}\rangle) \tag{53}$$

where N_{Tr} is the number of tubes in transverse direction, S_{Tr} is the dimensionless transverse distance between two consecutive tubes, N_D is the number of total tubes and $\langle \tilde{T}_{out}\rangle$ is the average dimensionless temperature at the outflow boundary.

Table 2 shows the comparison of the present average Nusselt number with previous empirical correlations. Present result is about 10% higher than the result of Grimison [8] and about 18% higher than the result of Zukauskas [1]. Considering the accuracy of about 25% of the empirical correlations [9], the agreement of the average Nusselt number is good.

The local Nusselt number distribution along the tubes surface is shown in Fig. 12a where the tube numbers are marked in Fig. 11. Interestingly, the local Nusselt number distributions on the tubes from the second to the ninth are almost the same after the transfer calculation by Eq. (54) as shown in Fig. 12b. The local Nusselt number distribution on the mth tube's surface can be written as:

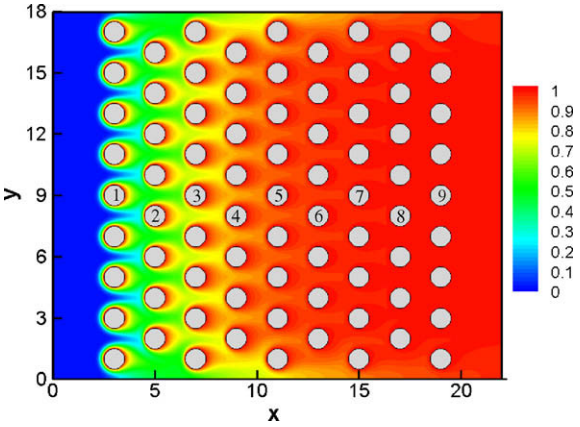

Fig. 11. Distribution of temperature field for the case of flow past a staggered tube bank with heat transfer at Re = 20.

Table 2
Comparison of the average Nusselt number.

Authors	Present	Grimison [8]	Zukauskas[1]
$\langle Nu \rangle$	4.08	3.71	3.45

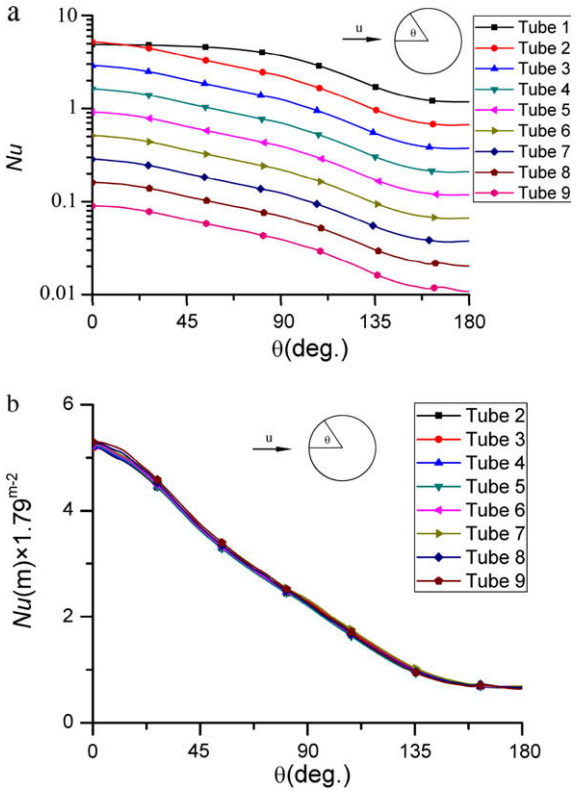

Fig. 12. Local Nusselt number distribution along the tubes surface where the tube numbers are marked in Fig 11: (a) from the first tube to the ninth tube; (b) from the second tube to the ninth tube after the transfer equation $Nu(\theta,m) = Nu(\theta,2) \times 1.79^{2-m} (m \geq 2)$.

$$Nu(\theta,m) = Nu(\theta,2) \times 1.79^{2-m}, \quad m \geq 2 \tag{54}$$

or more general, we can get

$$Nu(\theta,m_1) = Nu(\theta,m_2) \times 1.79^{m_2-m_1}, \quad m_1 \geq 2, \ \ m_2 \geq 2 \tag{55}$$

where $Nu(\theta,m)$ is the Nusselt number at the θ position on the mth tube's surface.

4. Summary and conclusion

In the present paper, the immersed boundary method with finite difference scheme is extended to solve heat transfer problem. A direct heat source scheme is proposed to let the temperature at the immersed boundary satisfied the temperature Dirichlet boundary condition. And the explicit interactive process of the direct heat source scheme called multi-direct heat source scheme is applied to ensure the satisfaction of the temperature Dirichlet boundary condition at the immersed boundary. The second-order spacial accuracy of the solver has been confirmed by simulating the Taylor–Green vortices. The simulations of natural convection between concentric cylinders, and flow past a stationary circular cylinder have been conducted to validate the accuracy of present method on solving heat transfer problems. And at last, the computation of flow past a staggered tube bank with heat transfer has been

done to verify the capability of present method on solving complex geometries problems.

The main advantage of the multi-direct forcing/heat source scheme is that the error between the calculated value of velocity/temperature and the desired velocity/temperature at the immersed boundary are decreased when applies the multi-direct forcing/heat source scheme. And this has been validated through the calculation of the Taylor–Green vortices and the natural convection between concentric cylinders.

Acknowledgements

This work is supported by the National Natural Science Foundation of China (Nos. 50736006 and 50776080) and the National High Technology Research and Development of China 863 Program (2007 AA05Z254). We are grateful to that.

References

[1] A. Zhukauskas, Heat transfer from tubes in cross flow, in: J.P. Hartnett, T.F. Irvine Jr. (Eds.), Advances in Heat Transfer, vol. 8, Academic Press, New York, 1972, pp. 93–160.
[2] M.W. Chang, B.A. Finlayson, Heat transfer in flow past cylinders at Re < 150 – Part I. Calculations for constant fluid properties, Numer. Heat Transfer 12 (1987) 179–198.
[3] H.S. Yoon, J.B. Lee, H.H. Chun, A numerical study on the fluid flow and heat transfer around a circular cylinder near a moving wall, Int. J. Heat Mass Transfer 50 (2007) 3507–3520.
[4] J. Kim, D. Kim, H. Choi, An immersed-boundary finite volume method for simulations of flow in complex geometries, J. Comput. Phys. 171 (2001) 132–150.
[5] J.L. Rosales, A. Ortega, J.A.C. Humphrey, A numerical investigation of the convective heat transfer in unsteady laminar flow past a single and tandem pair of square cylinders in a channel, Numer. Heat Transfer Part A 38 (2000) 443–465.
[6] S.V. Garimella, P.A. Eibeck, Onset of transition in the flow over a three-dimensional array of rectangular obstacles, Trans. ASME J. Electron. Packag. 114 (1992) 251–255.
[7] P. Bagchi, M.Y. Ha, S. Balachandar, Direct numerical simulation of flow and heat transfer from a sphere in a uniform cross-flow, Trans. ASME J. Fluids Eng. 123 (2001) 347–358.
[8] E.D. Grimison, Correlation and utilization of new data on flow resistance and heat transfer for cross flow of gases over tube banks, Trans. ASME 59 (1937) 583–584.
[9] J.P. Holman, Heat Transfer, ninth ed., McGraw-Hill, 2002. pp. 291–296.
[10] B.S. Kim, D.S. Lee, M.Y. Ha, H.S. Yoon, A numerical study of natural convection in a square enclosure with a circular cylinder at different vertical locations, Int. J. Heat Mass Transfer 51 (2008) 1888–1906.
[11] Z.G. Feng, E.E. Michaelides, Heat transfer in particulate flows with direct numerical simulation, Int. J. Heat Mass Transfer 52 (2009) 777–786.
[12] R. Glowinski, T.W. Pan, T.I. Hesla, D.D. Joseph, A distributed Lagrange multiplier/fictitious domain method for particulate flows, Int. J. Multiphase Flow 25 (1999) 755–794.
[13] S. Xu, Z.J. Wang, An immersed interface method for simulating the interaction of a fluid with moving boundaries, J. Comput. Phys. 216 (2006) 454–493.
[14] C.S. Peskin, Flow patterns around heart valves: a numerical method, J. Comput. Phys. 10 (1972) 252–271.
[15] R. Mittal, G. Iaccarino, Immersed boundary methods, Annu. Rev. Fluid Mech. 37 (2005) 239–261.
[16] D. Goldstein, R. Handler, L. Sirovich, Modeling a no-slip boundary with an external force field, J. Comput. Phys. 105 (1993) 354–366.
[17] E.M. Saiki, S. Biringen, Numerical simulation of a cylinder in uniform flow: application of a virtual boundary method, J. Comput. Phys. 123 (1996) 450–465.
[18] E.A. Fadlun, R. Verzicco, P. Orlandi, J. Mohd-Yusof, Combined immersed-boundary finite-difference methods for three-dimensional complex flow simulations, J. Comput. Phys. 161 (2000) 35–60.
[19] M. Uhlmann, An immersed boundary method with direct forcing for the simulation of particulate flows, J. Comput. Phys. 209 (2005) 448–476.
[20] Z. Wang, J. Fan, K. Luo, Combined multi-direct forcing and immersed boundary method for simulating flows with moving particles, Int. J. Multiphase Flow 34 (2008) 283–302.
[21] A.L.F.L.E. Silva, A. Silveira-Neto, J.J.R. Damasceno, Numerical simulation of two-dimensional flows over a circular cylinder using the immersed boundary method, J. Comput. Phys. 189 (2003) 351–370.
[22] B.E. Griffith, C.S. Peskin, On the order of accuracy of the immersed boundary method: higher order convergence rates for sufficiently smooth problems, J. Comput. Phys. 208 (2005) 75–105.
[23] S.K. Lele, Compact finite difference scheme with spectral-like resolution, J. Comput. Phys. 103 (1992) 16–42.
[24] A. Jameson, W. Schmidt, Some recent development in numerical methods for transonic flow, Comput. Methods Appl. Mech. Eng. 51 (1985) 467–493.
[25] K. Luo, Z. Wang, J. Fan, K. Cen, Full-scale solutions to particle-laden flows: multidirect forcing and immersed boundary method, Phys. Rev. E 76 (2007) 066709.
[26] S.C.R. Dennis, G.Z. Chang, Numerical solution for steady flow past a circular cylinder at Reynolds number up to 100, J. Fluid Mech. 42 (1970) 471–489.
[27] T. Ye, R. Mittal, H.S. Udaykumar, W. Shyy, An accurate Cartesian grid method for viscous incompressible flows with complex immersed boundaries, J. Comput. Phys. 156 (1999) 209–240.
[28] T.H. Kuehn, R.J. Goldstein, An experimental and theoretical study of natural convection in the annulus between horizontal concentric cylinders, J. Fluid Mech. 74 (1976) 695–719.
[29] H. Gan, J. Chang, J.J. Feng, H.H. Hu, Direct numerical simulation of the sedimentation of solid particles with thermal convection, J. Fluid Mech. 481 (2003) 385–411.
[30] S.C.R. Dennis, J.D. Hudson, N. Smith, Steady laminar forced convection from a circular cylinder at low Reynolds number, Phys. Fluids 11 (1968) 933–940.
[31] I. Orlanski, A simple boundary condition for unbounded hyperbolic flow, J. Comput. Phys. 21 (1976) 251–269.
[32] D.J. Tritton, Experiments on the flow past a circular cylinder at low Reynolds number, J. Fluid Mech. 6 (1959) 547–567.